Aerospace Science and Technology 71 (2017) 382–391

Contents lists available at ScienceDirect

Aerospace Science and Technology

www.elsevier.com/locate/aescte

An investigation on the effect of pitchwise endwall design in a turbine cascade at different incidence angles

K.N. Kiran, S. Anish *

Turbomachinery Laboratory, Department of Mechanical Engineering, National Institute of Technology Karnataka, Mangalore-575025, India

ARTICLE INFO

Article history:
Received 21 April 2017
Received in revised form 19 September 2017
Accepted 19 September 2017
Available online 25 September 2017

Keywords:
Endwall profile
Secondary flows
Horseshoe vortex
Gas turbine
Turbine cascade

ABSTRACT

This paper describes the effects of non-axisymmetric endwall profiling on the aerodynamic performance of a linear turbine cascade at different incidence angles. The sinusoidal profiling is carried out with constant profile curvature along the mean streamline path. Three different profiles, with varying hump to dip height, are analyzed numerically and the performances are compared with the planar profile. Reynolds Averaged Navier Stokes (RANS) equations are solved in their conservative form using Finite Volume Method with SST turbulence model. The calculated results indicate that the profiled endwall minimizes the lateral movement of weaker boundary layer fluid from the hub-pressure side corner. In comparison with planar case, the flow deviations are largely contained with endwall profiling but closer to the endwall it enhances the overturning and secondary flow kinetic energy. The reduction in loss coefficient is estimated to be 1.3%, 8.7% and 38% for incidence angles of $-10°$, nominal and $+15°$ respectively. The sinusoidal profiling has brought down the pitch averaged flow deviation and secondary flow kinetic energy at nominal and positive incidence angles but the impact is insignificant at negative incidence. Profiling minimizes the rolling up of the passage vortex and makes the passage vortex to migrate closer to the endwall. This flow modification brings down the losses in the core flow but enhances the losses near the endwall.

© 2017 Elsevier Masson SAS. All rights reserved.

1. Introduction

In any gas turbine about 33% of the total losses are attributed to secondary flow losses [1]. Secondary flows refer to three-dimensional, vortical flow structures that develop in turbine vane and blade passages due to high turning of the flow and non-uniform inlet total pressure profiles. Sieverding [2] gives the comprehensive description of experimental secondary flow features and effect of boundary layer in a straight turbine cascade. Numerous experimental and theoretical works have been reported and the behavior of secondary flows and its influence on the turbine performance are almost well understood. Out of various methods (filleting the leading edge, fencing the blade passage, endwall profiling, blade lean and blade thickening) suggested for reducing the secondary flow losses, endwall profiling emerged as a viable and effective mechanism.

In general, the endwall profiling is achieved either by axial profiling along the passage with no pitchwise variation or non-axisymmetric profiling along the passage with profile variations in both the axial and pitchwise directions. The profiling is aimed either to accelerate the boundary layer fluid at the endwall or to reduce the pitchwise pressure gradient at the endwall. Harvey et al. [3] carried out non-axisymmetric endwall profiling to reduce the passage vortex strength which causes an increase in exit angle deviation. Normally underturning occurs away from the wall while overturning appears near the endwall. By controlling the lateral pressure gradient, overturning near the endwall can be minimized and this is made possible by providing streamline curvature. The profiled endwall gives less rolling up of boundary layer and convection of high energy fluid when compared with planar endwall [4]. Also it gives significantly less angle variation at exit and reduces secondary kinetic energy. The profiling reduces the cross passage pressure gradient in the blade row by the action of streamline curvature. It was found that the inlet boundary layer locally separates on the suction surface of passage, generating extra losses which feeds directly into the core of passage vortex [5]. Ingram et al. [5] found 31% reduction in the secondary loss for profiled endwall in comparison with planar case. Though they observed performance enhancement via experimental methods the computational results failed to predict the loss prediction qualitatively and quantitatively.

For designing of the endwall several procedures have been put into practice. Rose [6] used a streamline curvature in the radial

* Corresponding author.
E-mail address: anish@nitk.edu.in (S. Anish).

https://doi.org/10.1016/j.ast.2017.09.032
1270-9638/© 2017 Elsevier Masson SAS. All rights reserved.

Nomenclature

A	Profile amplitude	m	
C_{ax}	Axial chord	m	
C_{P0}	Total pressure loss coefficient		
C_P	Static pressure loss coefficient		
H_p	Pressure side leg horseshoe vortex		
i	Incidence angle	Deg	
P	Static pressure	N/m^2	
P_0	Total pressure	N/m^2	
Re	Reynolds number		
S	Blade span	m	
S_p	Suction side leg horseshoe vortex		
T	Transverse blade pitch		
V	Velocity	m/s	
V_u	Axial velocity	m/s	
V_v	Tangential velocity	m/s	
V_w	Radial velocity	m/s	

Symbols

α	Exit flow angle	degrees
ρ	Density	kg/m^3
ξ	Zeta	

Subscripts and superscripts

1	Inlet of cascade
2	Outlet of cascade
$-$	Pitchwise mass averaged quantity
$=$	Mass averaged quantity

direction to counteract accelerations in the circumferential direction and observed a 70% reduction in the non-uniformities. Harvey et al. [3] designed the endwall using b-spline curves that run through circumferential and axial directions and optimized the performance in terms of secondary kinetic energy and overturning near the endwall. Brennan et al. [7] redesigned the HP turbine of Rolls-Royce Trent 500 engine using a forward and inverse 3D design method. The profile shape was determined by six control points fixed at different axial locations. A sinusoidal shape may be generated at these locations and a surface is fitted over six b-splines. The predicted reduction in secondary loss was by 0.24% of stage efficiency for nozzle and by 0.16% for the rotor. More recent developments shows the three dimensional endwall designs via automatic optimization process for maximizing stage efficiency [8] and [9]. The combination of endwall contouring and leading edge filleting was tested in a turbine NGV by Turgut and Camci [10,11].

Much of the optimized profile designs were based on analysis made with a certain set of operating parameters. The suitability of the designed endwall profile at different operating conditions have been overlooked in many cases. Ideally, the designed endwall must satisfactorily work for various operating conditions of the turbine. The objective of the present work is to quantify the effect of endwall profiling on secondary flow losses in a linear turbine cascade under various incidence angles. Variations in the exit flow deviation as well as the secondary flow kinetic energy are also brought under the scope of this investigation.

2. Methodology

In the present investigation a linear turbine cascade (Durham Cascade) has been chosen. The Durham cascade is a low speed, large scale linear cascade for a high pressure rotor design. The blades are designed to have an aerodynamic similarity same as real machines rather than geometrical similarity [12]. It operates at a Reynolds number several times lower than a real turbine. The blade profile and geometrical details are given in Table 1. The Durham cascade has already been subjected to numerous study on endwall contouring and filleting in the past. Flow separations are more dominant in highly cambered blades, which is the reason behind selecting this cascade.

3. Geometrical modeling and meshing

The geometrical modeling and meshing of the computational domain is carried out using ICEM CFD. The inlet of the fluid domain is 1.5 times the axial chord distance (C_{ax}) away from the leading edge of the blade. The outlet plane is kept at a distance of two times the axial chord distance away from the trailing edge of the blade. In order to reduce the computational effort and time, only half of the span is modeled by specifying symmetric wall condition at the midspan region. Along the transverse direction, translational periodicity is set at one pitch length (Fig. 1a). The mesh around the blade and hub surface are fully structured and remaining flow domain is unstructured in axial and tangential direction. The maximum grid element size for whole domain is 3.5 mm with scale factor of 1. Fine prism layers are attached around the blade and hub surface to take care of the boundary layer effects (Fig. 1b). The first cell height normal to the surface is 0.35 mm with exponential height ratio of 1.15 up to 12 layers.

Table 1
Cascade blade details.

Blade inlet angle	47.6°
Blade exit angle	−68.0°
Stagger angle	−36.1°
Blade chord	224 mm
Axial chord	181 mm
Blade pitch, B	191 mm
Blade span, S	400 mm
Reynolds number (based on axial chord and exit velocity)	4.3×10^5
Exit Mach number	0.11

4. Solver details

The simulations are carried out with Reynolds Averaged Navier Stokes (RANS) equations using ANSYS-CFX. The RANS equations are solved in their conservative form using the Finite Volume Method. The inlet boundary conditions are as follows; total pressure profile is given at the inlet as shown in Fig. 2 with a turbulent intensity of 5%. The working fluid is air, as an ideal gas, which enters the domain with a static temperature of 292.15 K. At the outlet, fixed mass flow is specified for all the cases. The domain walls are specified with no slip condition and assumed to be perfectly insulated. High-resolution discretization scheme was chosen for all simulations and convergence criteria is set to 10^{-6}.

5. Design of endwall

In the present investigation three different sinusoidal endwall profile has been used and they are compared with planar case. Endwall profiles are derived from the following equation.

$$P_n = A * \sin\left[\frac{\pi (T - tc)}{w}\right] \quad (1)$$

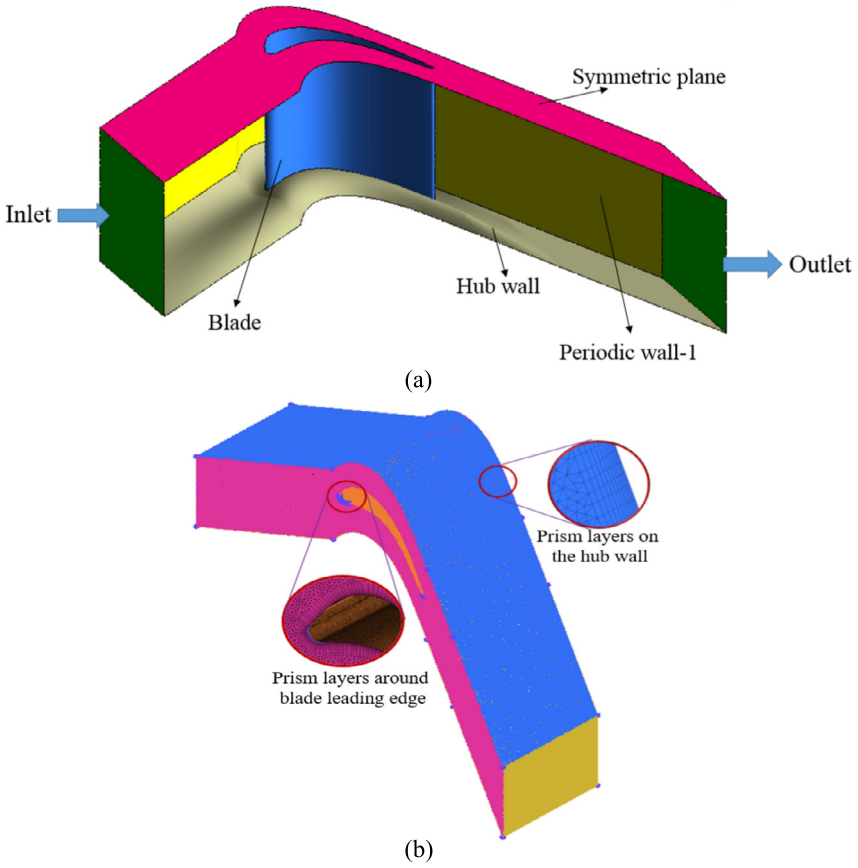

Fig. 1. (a) Computational domain listing all the boundaries. **(b)** Mesh generated for the domain (prism layers are zoomed in for better visibility).

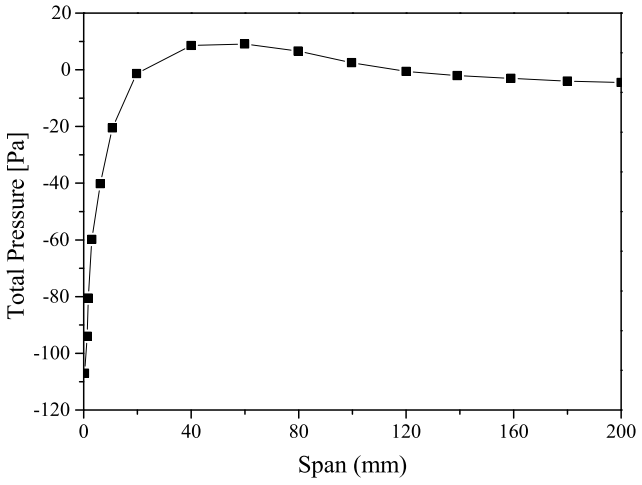

Fig. 2. Total pressure profile at inlet.

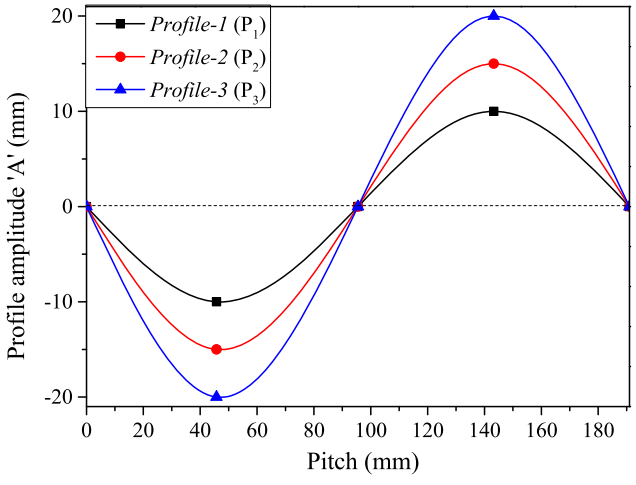

Fig. 3. The sinusoidal profile used for the endwall profile.

where, P_n is blade profile, A is profile amplitude in mm, w and tc are constant value corresponds to 95.5 mm, T is transverse pitch. Three different profiles are generated by varying the amplitude of the sine wave from 10 mm to 20 mm in steps of 5 mm. The generated profiles are named as *Profile*-1 (P_1), *Profile*-2 (P_2) and *Profile*-3 (P_3) respectively with increasing hump to dip heights (Fig. 3). The planar profile (*Base case*) is referred as (P_0). Non-axisymmetric profiling is carried out for one pitch length along the axial direction and the profile curvature remains invariant along the mean streamline curve. The three-dimensional surface profile for planar (P_0) and a profiled endwall (P_2) is shown in Fig. 4.

6. Verification and validation

The verification process examines the accuracy in the models through comparison to exact analytical results. Roache [13] identified that grid convergence studies are the most reliable technique for the quantification of numerical uncertainty. Grid independent study is carried out with total pressure ratio as the objective function. The number of mesh elements versus total pressure ratio is shown in Fig. 5 for planar case. There is no significant changes in the pressure ratio beyond 3.1 million elements hence it is chosen for further simulations. Similar studies have been undertaken for all the profiled endwall cases.

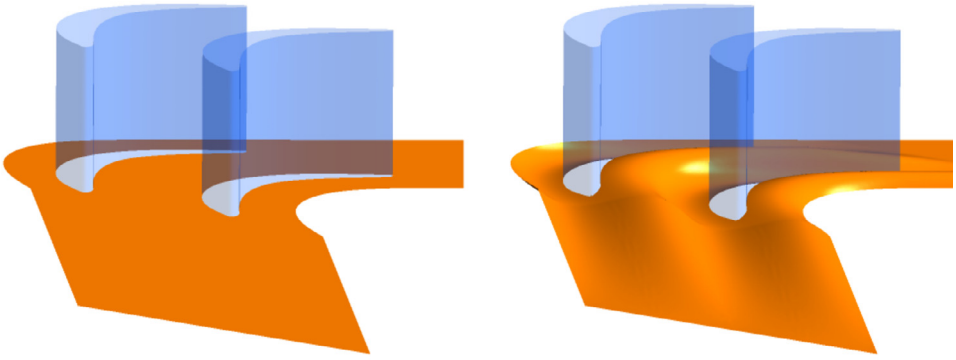

(a) Planar endwall (P_0) (b) Profiled endwall (P_2)

Fig. 4. Three-dimensional view of planar case and profiled endwall.

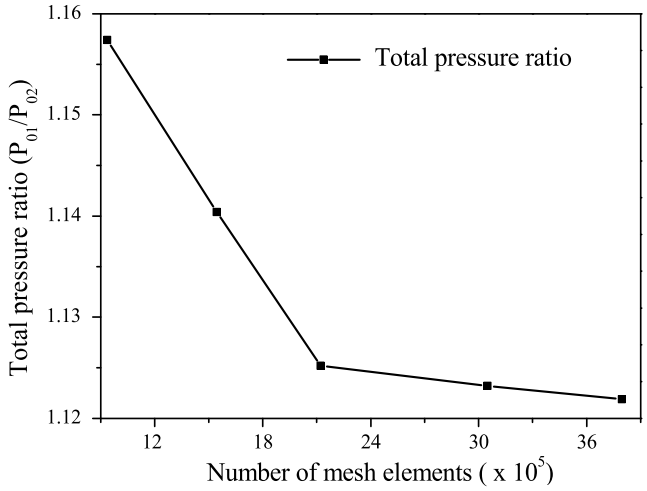

Fig. 5. Grid independence study for planar case.

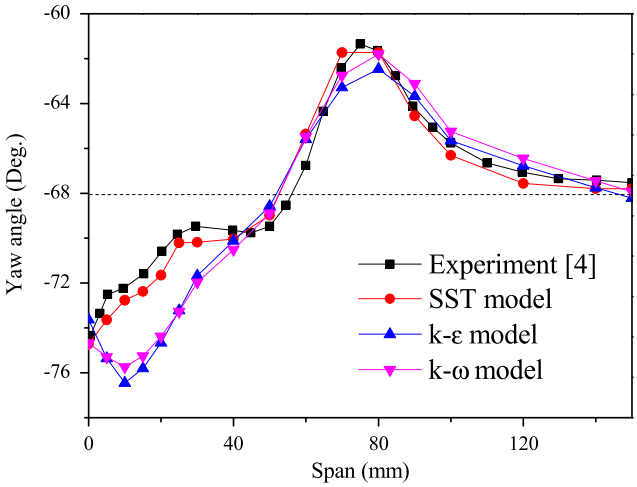

Fig. 6. Pitch averaged exit flow angle for Base case (P_0) at 128% C_{ax}.

For validation purpose the yaw angle variation in the span and the pitch averaged loss coefficient variations are considered and compared with the experimental results of Hartland et al. [4]. Fig. 6 shows the spanwise variation of yaw angle calculated at 128% C_{ax} for three different turbulence models. The shear stress transport (SST) model shows closer match to the experimental data than the standard k–ε and k–ω models. Hence the SST turbulence model has been selected for further analysis. It is noteworthy to mention that some of the previous studies also [14–16] identified the SST model as the most suitable turbulence model for analyzing secondary flows.

The total pressure loss coefficient is plotted at 9% C_{ax} distance before leading edge and at a downstream distance of 128% C_{ax} (Fig. 7a & b). The loss coefficients are evaluated from the hub wall to midspan in the following manner.

$$\overline{C_{po}} = \frac{\int V_u \xi dT}{\int V_u dT} \tag{2}$$

where,

$$\xi = \frac{P_{01} - P_0}{\rho V^2/2} \tag{3}$$

At the downstream side, the present numerical results are compared with the experimental and CFD results of Hartland et al. [4]. At the upstream location comparison is made only with the experimental data as CFD results of Hartland et al. [4] was not available for this location. Near to the endwall both CFD simulations are over predicting. From 10 mm span to 30 mm span, present CFD simulations are predicting better than numerical results of Hartland et al. [4]. From 30 mm span onwards the simulations are over predicting the loss coefficient values. This over prediction of loss coefficient may be attributed to several factors, the prominent being the transition nature of boundary layer near the endwall [17]. The RANS modeling assumes a fully turbulent boundary layer in place of a transitional boundary layer. Cui and Tucker [18] mentioned a new laminar boundary layer covers much of the endwall downstream of the pressure leg of the horseshoe vortex. Additionally, the separation from the blade surface is identified as an unsteady process with wide range of points of separation which are difficult to capture with RANS [18]. All these factors lead to an over prediction of the total pressure loss coefficient in RANS simulations. However, RANS simulations predicts the mean flow behavior with reasonable accuracy and it is very useful in predicting the overall performance analysis of the turbine blade. The present investigation is being a comparative study of different endwall profiles the focus is on the overall performance of the turbine cascade under different operating conditions.

7. Results and discussion

The flow modifications caused by the endwall profiling, in comparison with the planar case, are analyzed in this section. Particular emphasize is given on the loss coefficient variations, flow deviation and secondary flow kinetic energy. The effect of endwall profiling at different incidence angle is discussed at the latter part of this section.

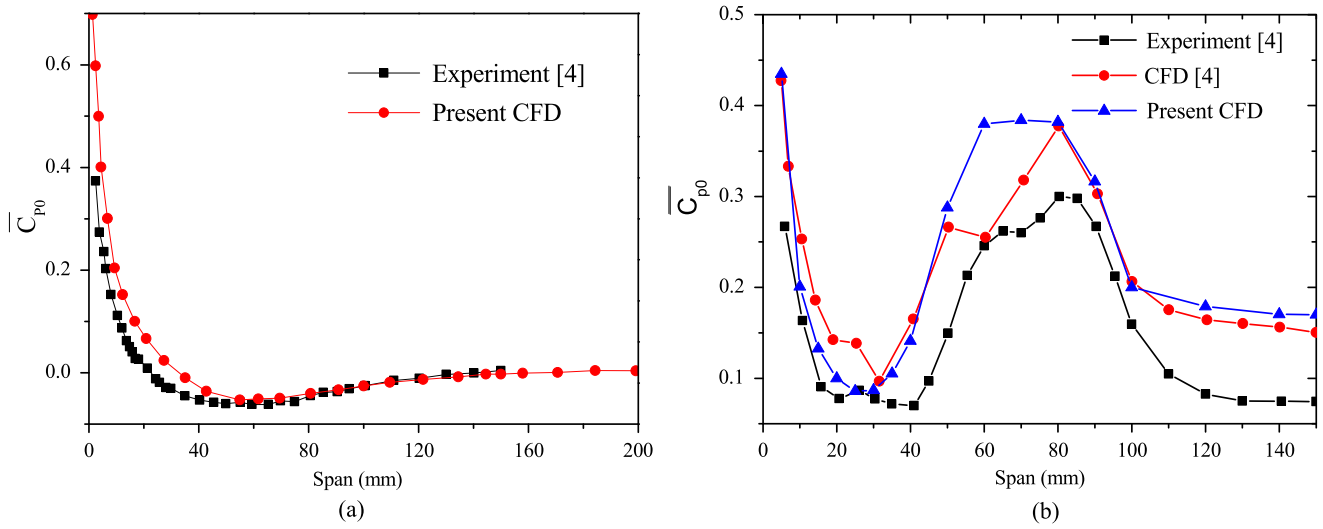

Fig. 7. Pitch averaged total pressure loss coefficient for base case (P_0) **(a)** at 9% C_{ax} before the leading edge and **(b)** at 128% C_{ax} downstream of the trailing edge.

8. Flow modifications in the turbine blade passage

Streamlines are generated from upstream of the leading edge to get an understanding about the flow behavior inside the blade passage. Fig. 8(a) shows streamlines in the blade passage superimposed on a total pressure contour plotted at 128% C_{ax}. The base case exhibits the classic horseshoe vortex pattern described by Sharma and Butler [19]. The passage vortex remain close the suction surface of the blade and it is driven toward the passage exit by the cross flow and pressure gradient along the passage. As the pressure side leg of horse shoe vortex is much larger and stronger compared to the suction side leg vortex, when they meet the sense of rotation of the passage is considered to be same as the rotation of the pressure side leg vortex. The downstream flow is distorted both in the spanwise and streamwise directions for the base case and the center of loss core region appears at a spanwise distance of 120 mm from the endwall.

When a sinusoidal profile has been given to the endwall, the center of the loss core region is shifted downwards to the endwall. For P_1 it appears at a span of 90 mm, at 81 mm for P_2 and at 67 mm for the P_3 profile. The rolling up of the passage vortex in the radial direction is subjected with the endwall profiling and the flow is less distorted at the exit region for profiled cases. However the profiling makes the passage vortex shifts closer to the endwall resulting into additional loss generation near the endwall.

To understand the reasons behind these flow modifications, it is imperative to analyze the flow behavior near the origin of passage vortex. The main purpose of endwall profiling is to bring down the pressure gradient in the pitchwise direction. This minimizes the lateral movement of weaker boundary layer fluid from the hub-pressure side corner (Fig. 9). The planar case shows a larger velocity gradient in the pitchwise direction. Near the endwall, the boundary layers are distorted and low momentum fluid is pushed towards the suction surface of the adjacent blade. Profiles P_2 and P_3 effectively prevent this crosswise movement of low momentum fluid.

9. Effect on total pressure loss coefficient

The pitch averaged total pressure loss coefficient ($\overline{C_{p0}}$), at a downstream distance of 128% axial chord (C_{ax}), is calculated for *Base case* and three endwall profile cases and are plotted in Fig. 10(a). For P_0, loss coefficient increases significantly from 20 mm to 120 mm of span due to the rolling up of the passage vortex. Due to the endwall boundary layer, the loss at the endwall is maximum. The loss coefficient is higher near the hub for profiled cases in comparison with planar case up to a span of 90 mm mainly due to the proximity of passage vortex close to the endwall. From a spanwise distance of 90 mm onwards there is a decrease in the value of loss coefficient for all profiled endwall. The intensity of passage vortex is smaller in the profiled endwall cases due to the delayed generation of passage vortex. For the planar case, the loss coefficient has increased significantly from 80 mm of span indicating migration of passage vortex from endwall to mean stream. Corresponding to the hump to dip height of the profile the $\overline{C_{P0}}$ values are also varying up to 120 mm of span beyond which the loss coefficients are similar for all the three endwall profiles. Among the three simulated cases, P_2 exhibits least value of loss coefficient. The peak value of $\overline{C_{P0}}$ corresponds to the center of loss core region.

Having observed the reduction of loss coefficient along the spanwise direction, the attention is focused on the variation of loss coefficient in the axial direction. The variation of mass averaged total pressure loss coefficient $\overline{\overline{C_{P0}}}$ has been plotted through different axial locations starting from 50% C_{ax} to 150% C_{ax} (Fig. 10 b). The variation of $\overline{\overline{C_{P0}}}$ along the axial direction is qualitatively similar for all the computations. It is observed that $\overline{\overline{C_{P0}}}$ increases significantly near the trailing edge of blade for all the simulated cases due to the trailing edge vortices and mixing of fluid from pressure and suction surface of blade. With the profiled endwall, the $\overline{\overline{C_{P0}}}$ variation is much more horizontal (smaller slope) than the base case. Similar to the spanwise variation, here also the loss coefficient attains a minimum value with *Profile-2*.

10. Effect on deviation and secondary kinetic energy

Near the endwall, velocity of fluid decreases in the boundary layer region and radius of curvature is less for boundary layer flow. There exists a pressure difference along the span which results in overturning in the passage flow. The overturning refers to larger flow deflection than expected geometrical deflection. Similarly, if flow deflection is less than geometrical deflection of blade, then it is referred as underturning. One of the primary objectives of endwall profile is to reduce underturning and overturning at the exit, which improves the performance of succeeding blade row.

Fig. 11 shows the exit flow deviation angle for all the simulated cases along the spanwise direction at 128% C_{ax}. Near the endwall overturning is observed for profiled endwall cases, which is in con-

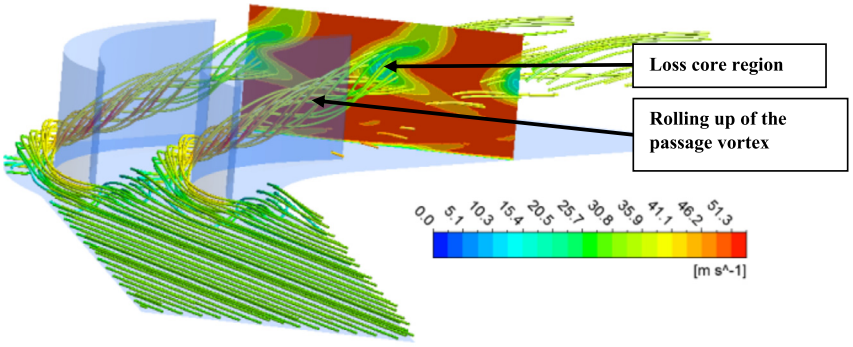

(a) *Base case* (P_0)

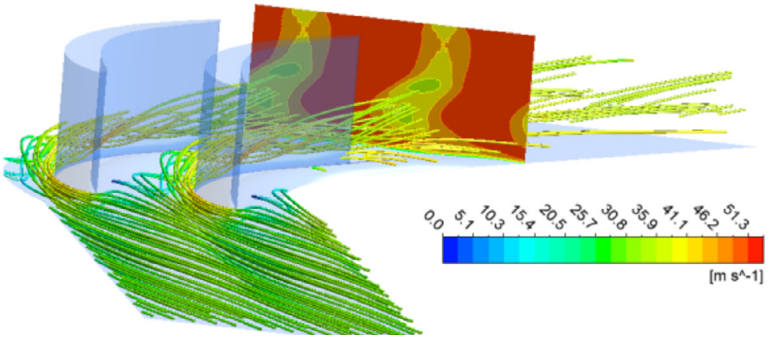

(b) *Profile-1* (P_1)

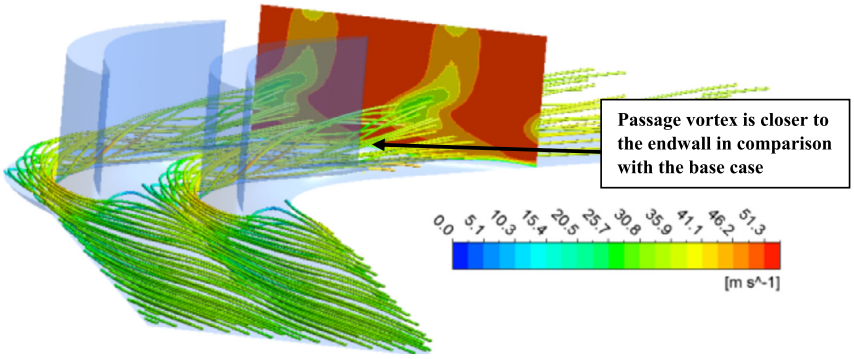

(c) *Profile-2* (P_2)

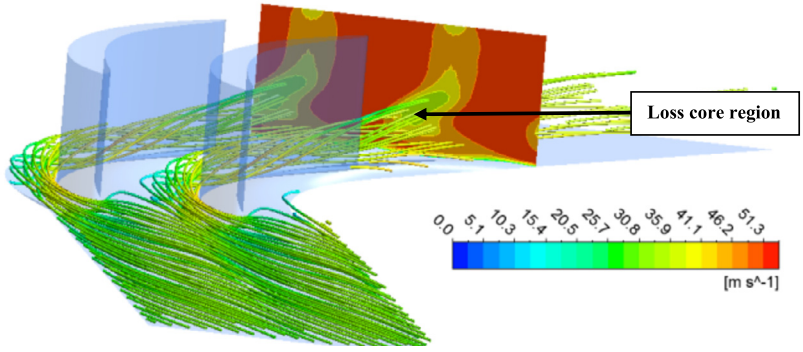

(d) *Profile-3* (P_3)

Fig. 8. Streamlines in the blade passage superimposed on a total pressure contour plotted at 128% C_{ax}. The loss core region is shifted downwards due to endwall profiling. (For interpretation of the colors in this figure, the reader is referred to the web version of this article.)

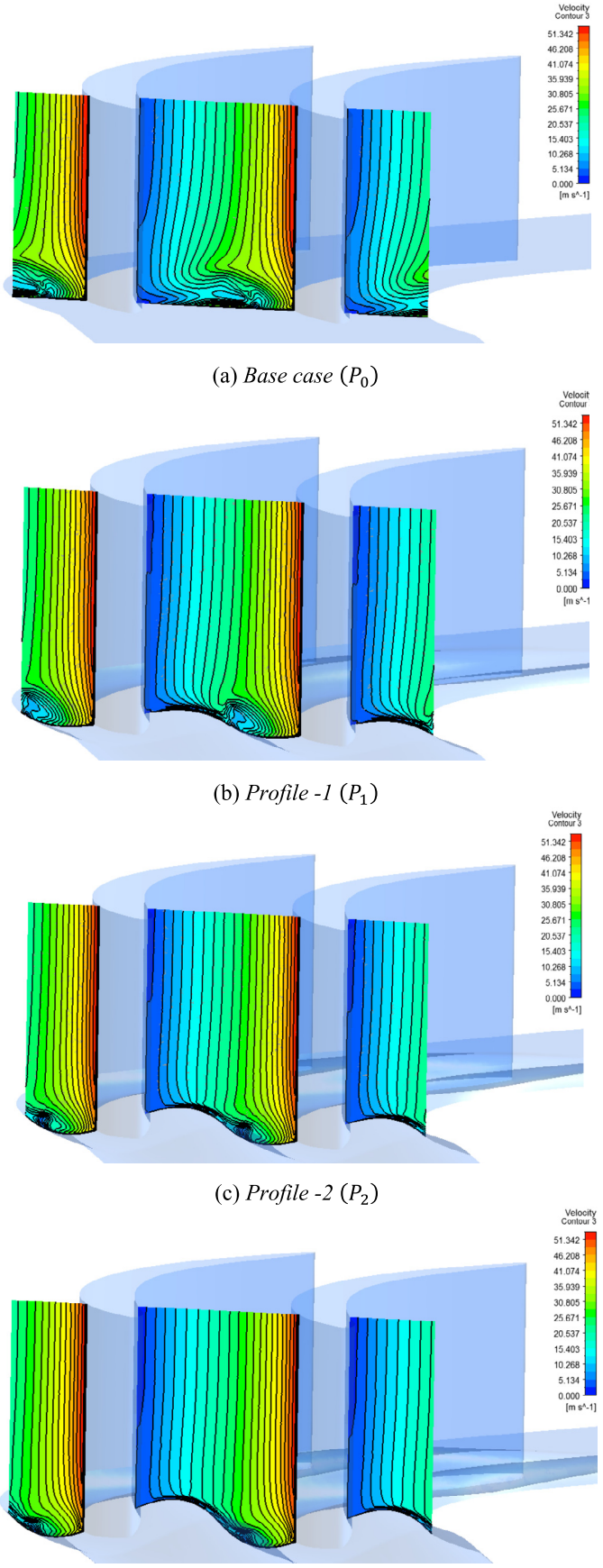

(a) *Base case* (P_0)

(b) *Profile -1* (P_1)

(c) *Profile -2* (P_2)

(d) *Profile -3* (P_3)

Fig. 9. Velocity contours inside the blade passage at 15% C_{ax}. (For interpretation of the colors in this figure, the reader is referred to the web version of this article.)

Table 2
Percentage deviation of mass averaged total pressure loss coefficient ($\overline{\overline{C_{P0}}}$) with the base case.

	Incidence angle					
	−10°	−5°	0°	+5°	+10°	+15°
Profile-1	−2.28%	−2.8%	−7.84%	−12.36%	−17.62%	−34.05%
Profile-2	−1.28%	−2.16%	−8.70%	−13.50%	−19.89%	−38.38%
Profile-3	+0.51%	−0.44%	−6.64%	−11.88%	−20.3%	−36.11%

trast with the flow angle of planar case. The flow pattern changes into underturning at spanwise distance of ∼40 mm for profiled cases. The planar profile exhibits underturning very close to the endwall but immediately shifts into overturning at span height of 12 mm. In comparison with base case the profiled endwall cases are showing less flow deviation, justifying the effectiveness of a uniform crest and trough profile in the circumferential direction. Closer to the endwall, the overturning is significantly high for the profiled cases probably due to the formation of corner vortex. The peak value for overturning has been reduced and its location has moved closer to the endwall. The direction of rotation of passage vortex is such that, below its center (i.e. near the endwall), it increases the tangential velocity of the fluid particles and above its center (away from the endwall) the tangential velocity decreases which results in an overturning. Among the profiled endwall cases, the *Profile-3* has lower overturning near the endwall but maximum underturning. This means, increasing the hump to dip distance helps in guiding the flow by reducing the deviation but away from the endwall it may results in a comparatively larger underturning. However in comparison with planar case the flow deviations are largely contained with the sinusoidal endwall profiling.

Secondary Kinetic Energy (SKE) at any plane measures vortices caused due to viscous effect and potential flow. For inviscid flow, SKE is proportional to the square of length of the vortex; i.e., when the mean flow increases, SKE of a streamwise vortex also increases [2]. The spanwise variation of Coefficient of Secondary Kinetic Energy (CSKE) exhibits a major reduction in secondary flow kinetic energy due to the endwall profiling and the peak CSKE has shifted towards the lower span (Fig. 12). This indicates that the profiling introduces additional secondary flows near the endwall. The profile P_2 has achieved a significant reduction in peak CSKE by 71% in comparison with base case.

11. Performance under different incidence angle

Investigations are carried out for different incidence angle for all profiled cases and compared with base case. The percentage deviation of mass averaged total pressure loss coefficient ($\overline{\overline{C_{P0}}}$) for different incidence angle in comparison with the base case is shown in Table 2. Negative sign indicates the percentage reduction in loss coefficient in comparison with base case. An analysis through these data indicates that the current sinusoidal endwall profiling is most favorable for positive incidence. The profile P_2 exhibits a 38% reduction on the mass averaged total pressure loss coefficient compared to base case at an incidence of +15°. On the contrary, at negative incidence angles the profiling does not reduce loss coefficient significantly. In fact at −10° incidence angle the losses are increasing slightly for *Profile-3*.

The exit flow angle deviation is also compared at different incidence angles measured at 128% C_{ax} and shown in Table 3. The percentage difference appears to be small due to the fact that the flow angle at this axial location is mass averaged and then compared with the blade exit angle. Local values of the percentage difference in flow deviations may be much higher than the average value. It is observed that percentage deviation is less for all the profiled cases in comparison with the base case. Among

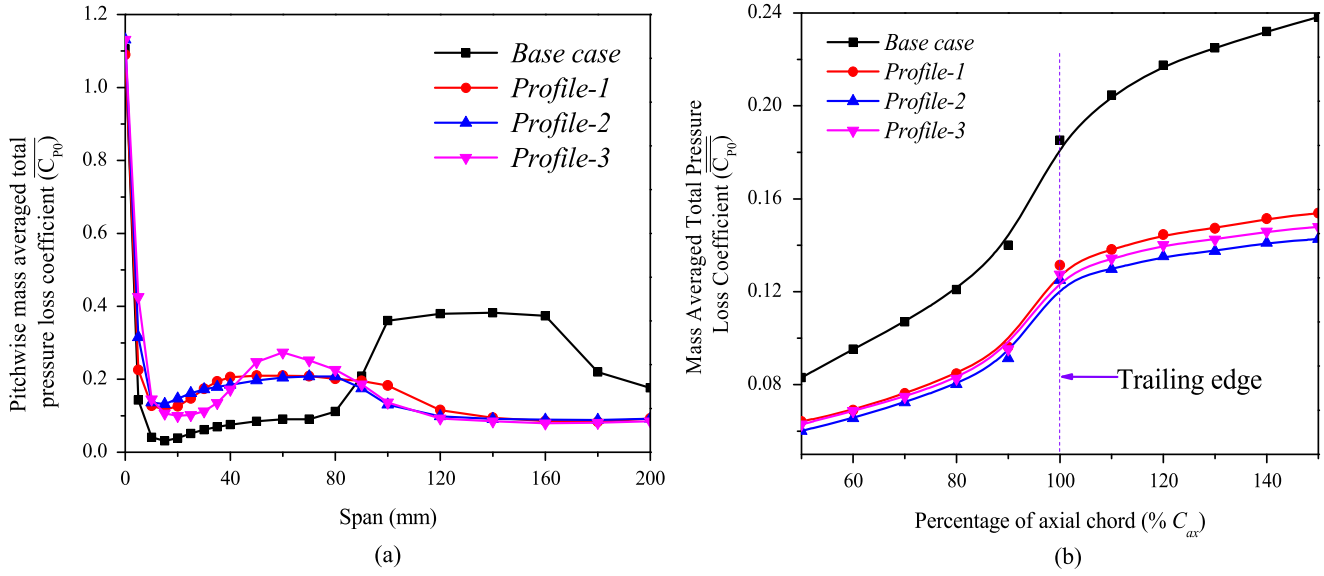

Fig. 10. Variation of **(a)** pitch-wise mass averaged total pressure loss coefficient ($\overline{C_{P0}}$) along the span. **(b)** Mass averaged total pressure loss coefficient ($\overline{\overline{C_{P0}}}$) along axial direction.

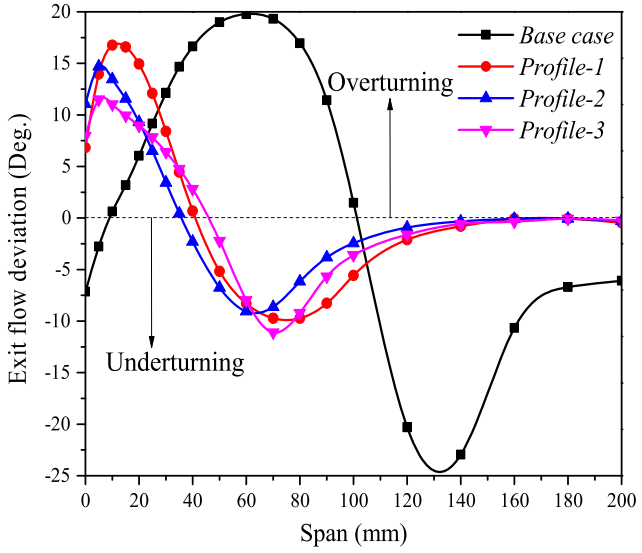

Fig. 11. Variation of pitchwise averaged exit flow angle deviation along the span.

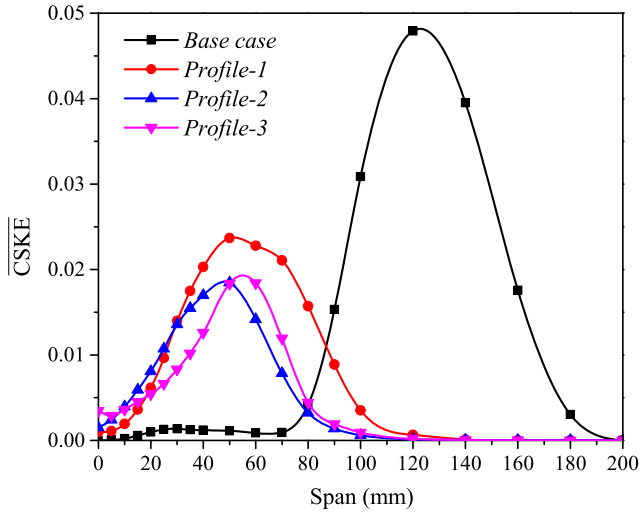

Fig. 12. Variation of pitchwise averaged coefficient of secondary kinetic energy (CSKE) along the span.

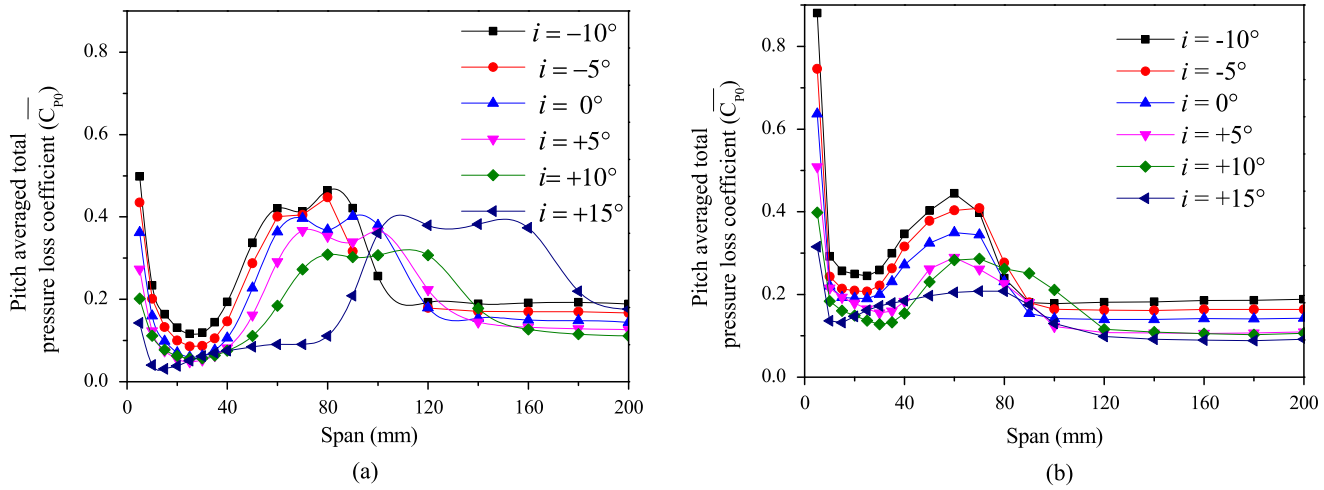

Fig. 13. Variation of pitch-wise mass averaged total pressure loss coefficient ($\overline{C_{P0}}$) at different incidence angle along the span: **(a)** *base case*, **(b)** *profile case* (P_2).

Table 3
Percentage deviation of mass averaged exit angle ($\bar{\bar{\alpha}}$) in comparison with exit blade angle.

	Incidence angle					
	−10°	−5°	0°	+5°	+10°	+15°
Profile-1	0.51%	0.64%	0.69%	0.89%	1.32%	1.91%
Profile-2	0.58%	0.69%	0.7%	0.75%	1.26%	1.47%
Profile-3	0.58%	0.70%	0.69%	0.76%	1.33%	1.39%

the profiled case the deviation is minimum for P_1 for all positive angle of incidence. Tables 2 and 3 show that the percentage improvement with the present profiling is beneficial mostly at high positive incidence angles and less advantageous at nominal and negative incidences.

To understand the poor performance of profiled endwall at negative incidences a detailed analysis was carried out for *Profile-2* at different incidence angles. Fig. 13 shows the pitch averaged total pressure loss coefficient for base case as well as *Profile-2*. Near the endwall positive incidence show moderate losses in comparison with the negative incidence cases (Fig. 13a). The loss coefficient follows a similar spanwise pattern for all incidence angles. However the peak loss coefficient is shifting along the span with increasing incidence angle. The shifting of this loss core region is observed primarily for the base case. For the profiled case, the movement of the loss core region along the spanwise direction is restricted. The profiling enhances losses near the endwall and for negative incidences the losses near the endwall are significantly higher than the positive incidence angles. To understand the flow behavior at negative incidence angle flow vectors are analyzed inside the blade passage.

Fig. 14 shows the velocity contours for base case and profiled cases at 15% C_{ax} within the blade passage. These contours has been plotted for one negative (−10°) and a positive incidence angle (+10°). The tangential velocity vectors are superimposed on these plots to understand the strength of the cross flow and also to identify the recirculation zones. The size of the flow vectors symbolizes their relative magnitude. For base case, at high positive incidence angle (+10°), the velocity gradient in the pitchwise direction is high and so will be the pressure gradient. Accordingly significant cross flows are observed from the suction side to pressure side which result into a strong recirculation zone near the endwall at high positive incidence angle (Fig. 14a). The profiling helps to reduce the cross flow and the recirculations near the endwall (Fig. 14b). On the contrary, the cross flow vectors are not stronger at negative incidence angle even for the base case. Consequently the profiling has no significant effect on the cross flows at negative incidence angles, but it is seen that the recirculation zone is pushed towards the hump region (hub-suction side corner). This cornering of the passage vortex may enhance the secondary flow kinetic energy near the endwall (as evident from Fig. 12) and this enhances the loss coefficient near the endwall. The profiling does help in reducing the losses in the mean stream flow, but at high negative incidence angle this reduction is not significant to surpass the enhancement of losses generated near the endwall. For positive incidence angles, the sinusoidal profile with constant profile curvature is highly beneficial.

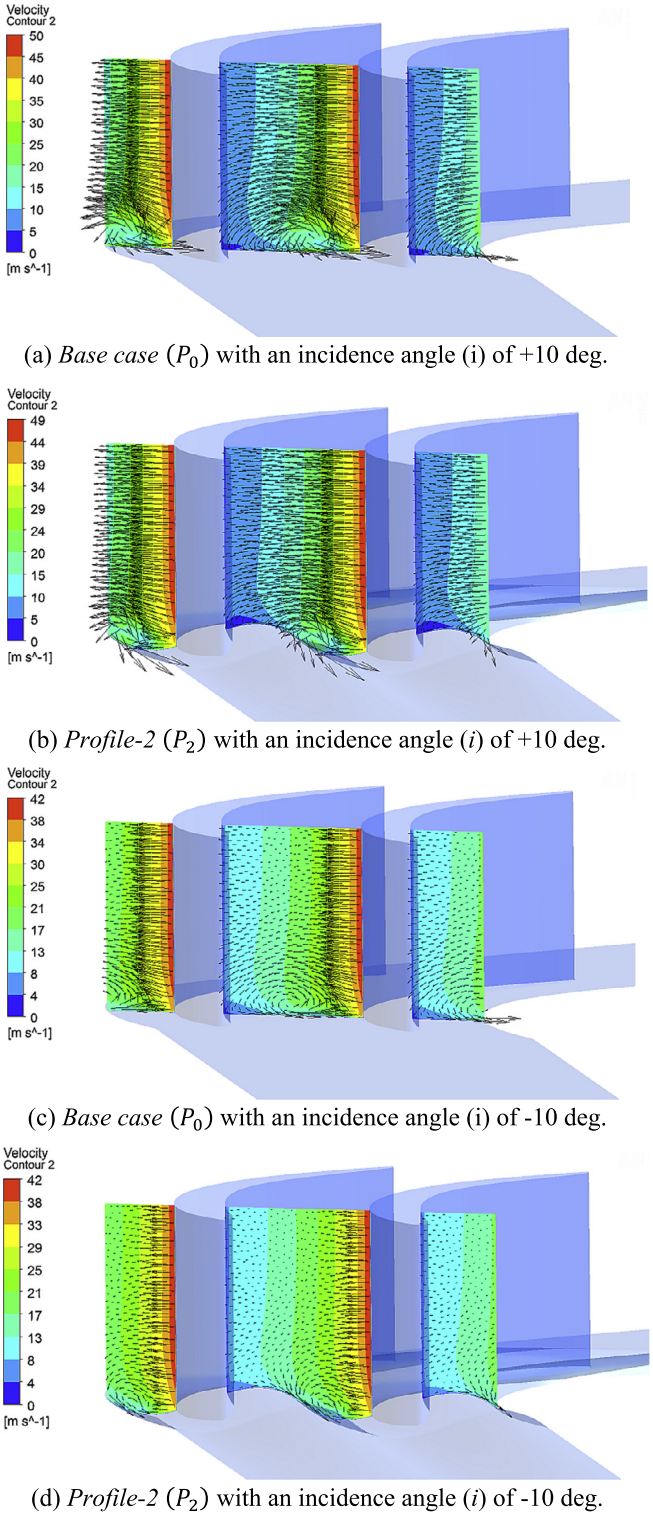

(a) *Base case* (P_0) with an incidence angle (i) of +10 deg.

(b) *Profile-2* (P_2) with an incidence angle (i) of +10 deg.

(c) *Base case* (P_0) with an incidence angle (i) of -10 deg.

(d) *Profile-2* (P_2) with an incidence angle (i) of -10 deg.

Fig. 14. Velocity contours in the blade passage at 15% C_{ax} superimposed with tangential component of velocity vector. (For interpretation of the colors in this figure, the reader is referred to the web version of this article.)

12. Conclusions

In the present numerical investigations, non-axisymmetric endwall profiling is carried out in a low pressure linear turbine cascade. Contrary to the conventional method, the profile curvature has been kept invariant along the mean streamline curve. Three different profiles, with varying hump to dip height, are analyzed and the performances were compared with the planar profile (*Base case*). Investigations are carried out at different incidence angles to understand the effect of sinusoidal endwall profile at different operating conditions. Following major conclusions are drawn from the analysis.

The designed endwall profiling helps to minimize the rolling up of the passage vortex in the radial direction which subsequently results in a lower flow distortion at the downstream. For planar profile the boundary layers are distorted and low momentum fluid

is pushed towards the suction surface of the adjacent blade. Profiled endwall effectively prevent this crosswise movement of low momentum fluid. Endwall profile with a larger hump to dip height, pushes the passage vortex closer to the endwall which generates additional losses near the endwall. This movement of the passage vortex results in a significant overturning closer to the endwall. However in comparison with planar case the flow deviations are largely contained with the endwall profiling. Beyond spanwise distance of 120 mm the flow deviations are almost negligible with profiled endwall and the secondary flow kinetic energy significantly reduces in the spanwise direction.

Analysis with different incidence angles reveals that the profiling is very effective at high positive incidence angles and almost insignificant at high negative incidence angles. The *Profile-2* exhibits 38% reduction on the mass averaged total pressure loss coefficient, compared to planar profile, at an incidence of $+15°$. On the contrary, at an incidence angle of $-10°$ the losses are increasing slightly (0.51%). The stronger cross flows and recirculations observed at high positive incidence angle are not visible for negative incidence. The cornering of the passage vortex, enhance the secondary flow kinetic energy near the endwall and for high negative incidence angle this results enhancing the total loss coefficient. Overall, the profiling does help in reducing the losses in the mean stream flow, but at high negative incidence angle this reduction is not significant to surpass the enhancement of losses generated near the endwall.

Conflict of interest statement

There are no conflicts of interest for the present work.

References

[1] J.D. Denton, Loss mechanisms in turbomachines, in: ASME International Gas Turbine and Aeroengine Congress and Exposition, 1993, V002T14.

[2] C.H. Sieverding, Recent progress in the understanding of basic aspects of secondary flows in turbine blade passages, J. Eng. Gas Turbines Power 107 (2) (1985) 248–257.

[3] N.W. Harvey, M.G. Rose, M.D. Taylor, S. Shahpar, J. Hartland, D.G. Gregory-Smith, Non-axisymmetric turbine end wall design, part I: three-dimensional linear design system, ASME J. Turbomach. 122 (2) (2000) 278–285.

[4] J.C. Hartland, D.G. Gregory-Smith, N.W. Harvey, M.G. Rose, Non-axisymmetric turbine end wall design: part II – experimental validation, in: ASME 1999 International Gas Turbine and Aeroengine Congress and Exhibition, 2000, V001T03A050.

[5] G. Ingram, D. Gregory-Smith, N. Harvey, Investigation of a novel secondary flow feature in a turbine cascade with end wall profiling, J. Turbomach. 127 (1) (2005) 209–214.

[6] M.G. Rose, Non-axisymmetric endwall profiling in the HP NGV's of an axial flow gas turbine, in: ASME, The Hague, Netherlands, 1994, GT1994-249.

[7] G. Brennan, N.W. Harvey, M.G. Rose, N. Fomison, M.D. Taylor, Improving the efficiency of the Trent 500-HP turbine using non-axisymmetric end walls, part I: turbine design, J. Turbomach. 125 (3) (2003) 497–504.

[8] Özhan H. Turgut, Cengiz Camcı, A nonaxisymmetric endwall design approach and its computational assessment in the NGV of an HP turbine stage, Aerosp. Sci. Technol. 47 (2015) 456–466.

[9] T. Poehler, J. Niewoehner, P. Jeschke, Y. Guendogdu, Investigation of non-axisymmetric endwall contouring and three-dimensional airfoil design in a 1.5-stage axial turbine – part I: design and novel numerical analysis method, J. Turbomach. 137 (8) (2015) 081009, 1–11.

[10] Ozhan H. Turgut, Cengiz Camcı, Experimental investigation and computational evaluation of contoured endwall and leading edge fillet configurations in a turbine NGV, in: Proceedings of ASME Turbo Expo, 2012.

[11] Özhan H. Turgut, C. Camci, Influence of Leading Edge Fillet and Nonaxisymmetric Contoured Endwall on Turbine NGV Exit Flow Structure and Interactions with the Rim Seal Flow, ASME Paper No. GT2013-95843, 2013.

[12] G.L. Ingram, Endwall Profiling for the Reduction of Secondary Flow in Turbines, Doctoral Dissertation, Durham University, England, 2003.

[13] P.J. Roache, Verification and Validation in Computational Science and Engineering, Hermosa Publishers, Albuquerque, New Mexico, 1998.

[14] D. Dunn, G.C. Snedden, T.W. Von Backström, Turbulence model comparisons for a low pressure 1.5 stage test turbine, in: 19th Conference of the International Society for Air Breathing Engines, Montreal, Quebec, Canada, 2009, 7 pp.

[15] K.N. Kumar, M. Govardhan, Secondary flow loss reduction in a turbine cascade with a linearly varied height streamwise endwall fence, Int. J. Rotating Mach. 15 (4) (2011) 296–305.

[16] Ozhan H. Turgut, Cengiz Camcı, A Nonaxisymmetric Endwall Design Methodology for Turbine Nozzle Guide Vanes and Its Computational Fluid Dynamics Evaluation, ASME Paper No. IMECE2011-64362, 2011.

[17] R. Mittal, S. Venkatasubramanian, F.M. Najjar, Large-eddy simulation of flow through a low-pressure turbine cascade, in: 15th AIAA Computational Fluid Dynamics Conference, Anaheim, CA, U.S.A., 2001.

[18] Jiahuan Cui, Paul Tucker, Numerical study of purge and secondary flows in a low-pressure turbine, J. Turbomach. 139 (2) (2016), http://dx.doi.org/10.1115/1.4034684, 021007-10.

[19] O.P. Sharma, T.L. Butler, Predictions of endwall losses and secondary flows in axial flow turbine cascades, in: ASME 1986 International Gas Turbine Conference and Exhibit, American Society of Mechanical Engineers, 1986, V001T01A098.